PCCP

Accepted Manuscript

This is an *Accepted Manuscript*, which has been through the Royal Society of Chemistry peer review process and has been accepted for publication.

Accepted Manuscripts are published online shortly after acceptance, before technical editing, formatting and proof reading. Using this free service, authors can make their results available to the community, in citable form, before we publish the edited article. We will replace this *Accepted Manuscript* with the edited and formatted *Advance Article* as soon as it is available.

You can find more information about *Accepted Manuscripts* in the **Information for Authors**.

Please note that technical editing may introduce minor changes to the text and/or graphics, which may alter content. The journal's standard **Terms & Conditions** and the **Ethical guidelines** still apply. In no event shall the Royal Society of Chemistry be held responsible for any errors or omissions in this *Accepted Manuscript* or any consequences arising from the use of any information it contains.

Adsorption studies of divalent, dinuclear coordination complexes as molecular spacers on SWCNTs

Jeffrey R. Alston,[a] David J. Banks,[a] Chauncey X. McNeill,[a] James B. Mitchell,[a] Leonid D. Popov,[b] Igor N. Shcherbakov,[b] and J. C. Poler[a†]

[a] Department of Chemistry, University of North Carolina at Charlotte, Charlotte, NC
[b] Chair of Physical and Colloid Chemistry, Southern Federal University, Rostov-on-Don, Russian Federation.

[a†] Corresponding Author: Department of Chemistry, University of North Carolina at Charlotte, Charlotte, NC Fax: (704) 687-0960; Tel: (704) 687-8289; E-mail: jcpoler@uncc.edu

† Electronic supplementary information (ESI†) available: 1. Molecular Structures of complexes studied, 2. UV-Vis-NIR spectra of +2Zn2 in dry DMF and DFT calculations of ion-paired complex in solution, 3. Electrophoretic mobility and zeta potential of SWCNTs, 4. Limiting molar conductivity, 5. Initial Rate of adsorption versus initial concentration, 6. adsorption isotherm data, 7. Molecular mechanics of SWCNT stability versus molecular spacer thickness, and 8. DFT calculations of ion-complex-SWCNT clusters.

Abstract

In order to enhance the electrical energy storage capabilities of nanostructured carbon materials, inter-particle spacer strategies are needed to maintain ion-accessible surface area between the nanoparticles. This paper presents a comparison between different classes of divalent, dinuclear coordination complexes which both show strong adsorption to SWCNTs and have molecular spacer properties that maintain electrochemical activity. We find that a novel, dinuclear zinc hydrazone complex binds as an ion-pair at very high loading while not inducing significant aggregation as compared to our previously studies of dinuclear ruthenium complexes. These conclusions are supported by conductivity and dispersion stability data. Moreover, since zinc is an earth abundant metal, these complexes can be used as components in sustainable energy storage materials. Binding kinetics and binding equilibrium data are presented. Modeling of the adsorption isotherm is best fit with the BET model. Kinetics data support an independent binding model. Preliminary capacitance and membrane resistance data are consistent with the complexes acting as molecular spacers between the SWCNTs in a condensed thin film.

1   Introduction

Nanomaterials are central to improving the performance of many technologies due to their high specific surface area (SSA) and stable surface characteristics. Directed assembly of these materials has led to enhanced energy conversion from dye sensitized solar cells[1]. Binding of petroleum additive molecules to the high surface area of these materials has enabled drinking water remediation.[2] One of the central challenges that most nanomaterials face is their unintended aggregation which drastically reduces the SSA. Combining nanomaterials of different shapes and sizes has led to improved energy storage supercapacitor performance.[3] Modifying the surface of a SWCNT can affect the external adsorption energy onto that SWCNT surface and alter the adsorption isotherm.[4] Many advances along this line of research have been reviewed recently.[5] Carbon nanotubes can be functionalized through physisorption[6-8] of molecular,[9] polymer,[10] or nucleic acid[11, 12] compounds. However these strategies are non-specific and tend to encapsulate the active surface of the nanostructured carbon, rendering it ineffective for electron transfer and ion adsorption.

In our recent work, we explored the long range interactions (LRI) between single-walled carbon nanotubes (SWCNTs) by probing the dispersed tubes with various solvated ionic species.[13] We showed that the stability of a dispersed nanostructured carbon material is dominated by Derjaguin, Landau, Verwey, and Overbeek (DLVO)[14, 15] type interactions and not structured solvent steric interactions. The species most effective at collapsing the electrical double layer (EDL) repulsion were dinuclear coordination complexes in which the bridging ligand mediated strong binding to the SWCNTs and acted as molecular spacers between them. In this paper, we present results on a new class of complex that binds to the SWCNTs as a molecular spacer, but does not collapse the EDL as effectively. This leads to significantly higher

loading of the electroactive complex onto the SWCNTs which may increase their utility as supercapacitor materials.

Here we compare the adsorption kinetics and adsorption equilibrium of two different divalent, dinuclear metal complexes. Adsorption of **+2Zn2** and **+2Ru2** can be understood through LRI such as van der Waals (vdW) forces, electrostatics, and π-π interactions. Electrostatic interactions are between the slightly negative surface charge present on the SWCNTs and the positive charge on the adsorbate. π-π interactions are present between the aromatic ligands present on both **+2Zn2**, **+2Ru2**, and the delocalized π-electrons on SWCNTs.[16] It has been previously reported that molecules containing greater aromatic moieties bind much more strongly to SWCNT surfaces than those species with less aromatic character.[17] Adsorption capacity onto SWCNTs surface is governed by the active binding sites available for adsorbates to bind and interact with.[18] Binding of **+2Ru2** to SWCNTs surface is considerably less than that of **+2Zn2** while the equilibrium constant for the former is larger due to the more extensive delocalization of the bridging ligand's frontier molecular orbitals.

2   Experimental

2.1 Sample Preparation

N,N-dimethylformamide (DMF) (Fisher, Spectranalyzed) was used as purchased, and kept dry under a $N_2(g)$ blanket, such that water contamination is below 1000 ppm. At this level of water contamination, LRI from hydration forces are insignificant, and are not considered in this study. Single-walled carbon nanotubes were HiPCO (Grade P CNT from CNI, now Unidym, 0.8–1.2 nm diameter, 100–1000 nm length). SWCNT dispersions were prepared by adding DMF (30 mL) to powder (0.5 mg) then tip ultrasonicated without temperature or gas environment

regulation for 30 min at 10 W RMS using a Fisher Scientific Sonic Dismembrator 60 (1/8" tip ultrasonicator). After ultrasonication, dispersions were ultracentrifuged using a Beckman Optima XL-100K at 20,000 g for 20 min to sediment any undispersed SWCNTs or carbonaceous material. The supernatant was removed carefully, then diluted to a final SWCNT concentration of ~10 mg L^{-1} as measured by NIR spectroscopy at $\lambda = 1025$ nm.[19] Samples were ultrasonicated an additional 20 min to ensure excellent dispersion immediately before use. All experiments were done at room temperature 18 °C - 20 °C unless otherwise specified.

2.2 Molecular spacers

Two metal coordination complexes were adsorbed to the SWCNTs as potential molecular spacers. A dinuclear ruthenium coordination complex, [Cl(2,2' ;6' ,2"-terpyridine)Ru(tetrapyrido[3,2- α:2' ,3' -c:3",2"-h:2",3"-j]phenazine)Ru(2,2' ;6' ,2"-terpyridine)Cl](PF$_6$)$_2$ (**+2Ru2**)[20] and a dinuclear zinc coordination complex, 4-(tert-butyl)-2,6-bis((2-(phthalazin-1-yl)hydrazono)methyl)phenol (m$_2$-methoxo) dizinc(II)-acetate (**+2Zn2**)[21] were dissolved in dry DMF for all binding studies. Molecular structures of these complexes are shown in Fig. S.1-2 in the Electronic Supplementary Information (ESI†). Two other complexes were rejected from this study due to their poor binding characteristics to SWCNTs. The complex 4-(*tert*-butyl)-2,6-bis((2-(4,5-dihydro-1H-imidazol-2-yl)hydrazono)methyl)phenolate dicopper(II) dibromide[22] was used because Cu is an earth abundant metal, and the ligands had some aromaticity while the *tert*-butyl moiety has sufficient bulkiness to act as a spacer. The complex N'-(3,5-di-tert-butyl-2-hydroxybenzylidene)stearohydrazide copper(II) perchlorate[23] was chosen for study to see if the long alkyl chain would stabilize the complex to the nanotube. There was no significant adsorption by either complex and therefore they were not included in this study. Adsorbate concentrations were measured in dry DMF by UV-Vis-NIR spectroscopy.

Molar extinction coefficient $\varepsilon_{420} = 38700 \pm 400$ M^{-1}cm^{-1} (all results reported as value $\pm$ standard error, 95%) at $\lambda = 420$ nm was determined by method of standard dilutions. Representative spectra shown in Fig. S3A (ESI†). Absorbance versus concentration was linear from 0.1 μM to 10 μM. No evidence of complex dimerization was observed. These complexes do not absorb where we measure the SWCNT concentrations, at 1,025 nm.

2.3 Aggregation Kinetics

Aggregation kinetics of SWCNT dispersions upon the addition of the molecular adsorbents above were measured. Samples were prepared by adding adsorbent solutions of varying concentrations to SWCNT dispersions of constant concentration, 10 mg/l, and volume. Each sample was incubated in the dark for 48 h. At the low adsorbate concentration used, the dispersion is in the reaction limited colloid aggregation (RLCA) regime where aggregation rates are very slow. Samples were centrifuged at 10,000 g for 10 min in an Eppendorf 5415C tabletop centrifuge to sediment aggregated SWCNTs. The supernatant was immediately removed and analyzed by optical absorption spectroscopy. SWCNT concentration in the samples were normalized to a control containing no adsorbent. All measurements were performed in triplicates.

2.4 Conductivity

Electrical conductivity of the molecular adsorbents in DMF was performed. A Fisher Scientific Accumet AR20 (1.0 cm cell at 20 °C) was calibrated against a 0.340 M KCl standard, and the temperature dependent calibration was set to (2 %/°C). Samples were allowed to equilibrate for five minutes. The probe was rinsed in DMF between each measurement.

2.5 EDX

Energy dispersive x-ray spectroscopy (EDX) was performed on a JEOL- 6460LV, the accelerating voltage was set to 10 kV. Samples were prepared by drop-casting SWCNTs bound with **+2Zn2** onto silicon wafers. Elemental analysis of the samples was carried out. Atomic distribution of the elements carbon, nitrogen, zinc, and oxygen were analyzed for each sample.

2.6 Adsorption Studies and Binding Kinetics

Adsorption of molecular spacers to SWCNT surfaces were performed by adding various concentrations of adsorbent to the dispersion. Samples were prepared and allowed to incubate in polyallomer tubes for 2 or 5 hours. Adsorbates do not bind significantly (<1%) to the walls of the polyallomer tubes. Samples were ultracentrifuged in a Beckman Optima XL-100K at 100,000 g for 1 h, to ensure SWCNT aggregates do not interfere with optical absorption measurements. Immediately, the supernatant was pipetted off, and then the equilibrium concentration of unbound species was measured by optical absorption. Measured concentrations were normalized to a control SWCNT dispersion. Concentrations of molecular adsorbate were compared to initial controls to determine the quantity bound to SWCNTs. Similar studies were performed with incubation periods of 10 to 90 min increasing by 5 min intervals, to determine binding kinetics. The incubation time needed to reach the equilibrium concentration of adsorbate was determined from the adsorption kinetics too. The minimum incubation time of 10 min was limited by the time required to load samples into the rotor, pump down the ultracentrifuge, and then reach maximum RCF.

2.7 Zeta Potential

The electrophoretic mobility of SWCNT dispersions was measured using a Brookhaven Instruments Corporation Zeta-PALS system with operating voltage set to 10 V_{RMS}, and

measurements were performed at 25 °C. SWCNT dispersions of 2.72 mg/L in DMF were sonicated prior to measurement. Multiple runs were averaged after maximum and minimum outliers were discarded. Zeta potentials were calculated from the electrophoretic mobility using the Smoluchowski model.

2.8 DFT calculations

Density Functional Theory (DFT) was used to determine geometry optimization of the complex and the SWCNT. DFT calculations were completed with Materials Studio 4.4 (Accelrys) using a gradient corrected PBE functional. All core electrons were treated fully. A self-consistent field tolerance of 10^{-6} Ha and geometry optimization tolerance of 10^{-5} Ha were imposed with a maximum atom displacement of 0.005 Å (or a maximum force gradient of 0.002 Ha/Å). All optimizations were treated with a conductor-like screening model with a dielectric constant of 36.7 to simulate DMF, the solvent used for our electronic spectral studies to account for solvent interaction due to screening. All models are cluster calculation where the (7,7) SWCNT is terminated with H atoms to minimize the number of atoms (384 atoms in the complex-SWCNT calculation) and the computational expense. Orbital energies calculations are for qualitative assessment only as the PBE functional does not fully characterize the non-bonding LRI found in our systems.[24, 25]

2.9 Membrane Resistance

Membrane resistance measurements are made using vacuum filtration across a 9.55×10^{-4} m^2 0.272 mg thin film of SWCNTs. The flow rate of DMF through the membrane was measured

for successive 50.0 mL rinses. **+2Zn2** bound SWCNT films were made by incubating freshly

dispersed tubes in an initial concentration of the hydrazone complex for 90 min. The film was

formed onto a 0.45 µm pore polypropylene membrane and the filtrate was collected to determine

q, the amount of complex remaining after each DMF rinse.

3   Results and Discussion

3.1 Zeta potential of SWCNT dispersion

Zeta potential on the SWCNTs were measured to determine the change in surface potential upon

addition of adsorbate.[26] Phase analysis light scattering techniques are more sensitive to mobility

measurements in organic solvents such as DMF. Zeta potential measurements are used to

determine stability of EDL repulsion in SWCNT dispersion.[13] At higher zeta potential,

electrostatic repulsion will be greater, thus improving SWCNTs stability in DMF.[27] Increasing

charged adsorbent concentration (ionic strength) collapses the electrical double layer surrounding

the SWCNTs and aggregation will occur. Concentration of dispersion must be kept low to avoid

light induced aggregation from laser due to photophoresis.[28] Electrophetic mobility μ = -0.50 $\pm$

0.04 (10^{-8} m^2 V^{-1} s^{-1}) and zeta potential ζ= -12.4 $\pm$ 1 mV of pristine dispersion are consistent

with previous results.[13, 29] **+2Zn2** was added to the dispersion to a concentration of 6.25 µM.

The solution conductivity increased from 6 µS to 10 µS. As expected, the mobility and zeta

potential steadily decreased as soon as the molecular spacers were added and began to adsorb

onto the SWCNTs. After a few hours the mobility and zeta potential were stabilized at μ = -0.17

$\pm$ 0.02 (10^{-8} m^2 V^{-1} s^{-1}) and zeta potential ζ= -4.5 $\pm$ 0.5 mV as shown in Fig. S4 (ESI†).

3.2 Molar Conductivity and Degree of dissociation of molecular spacers

Onset of aggregation is useful in determining dispersion stability with various adsorbate and solvent systems. The **+2Ru2** species is fully dissociated in DMF; as described in previous work.[20] The **+2Zn2** acetate salt has a limiting molar conductivity $\Lambda_o = 24.7 \pm 0.4$ S cm^2 mol^{-1} as determined by fitting Ostwald's dilution law for weak electrolyte species, to the conductivity data.[30] The **+2Zn2** does not fully dissociate in DMF as expected for acetate salts in a solvent with dielectric constant of 35.6. These results are consistent with the strong ion paring interaction between Na$^+$ and C$_2$H$_3$O$_2^-$ ions in a DMF solution of sodium acetate. The limiting molar conductivity for sodium acetate in DMF is $\Lambda_o = 2.4 \pm 0.1$ S cm^2 mol^{-1} whereas the salt is fully dissociated in water with $\Lambda_o = 92.7 \pm 0.7$ S cm^2 mol^{-1} (data shown in Fig. S5 (ESI†)). The **+2Zn2** hydrazone exhibits a slightly higher limiting molar conductivity than sodium acetate in DMF. Since the **+2Zn2** hydrazone is an asymmetric ion there is an equilibrium of all three species [+2Zn2](Ac)$_2$, [+2Zn2](Ac)$^+$, and the [+2Zn2]$^{2+}$ at the concentrations used in this study. The most abundant species is the +1 ion-pair [+2Zn2](Ac)$^+$ as determined by fitting the conductivity data to Ostwald's dilution law for weak electrolytes as shown in Fig. 1. DFT Frontier molecular orbitals for the +1 ion-pair are shown in the inset of Fig. S3A. (ESI†). Additional orbitals for all three species are calculated and shown in Fig. S3B-D. (ESI†). The highest occupied orbitals reside on the acetate (blue-yellow) and the lowest unoccupied π orbitals reside on the ligand (green-red). This is consistent with an ion-pairing model of the dissolved species. From the orbitals and calculated energies it is likely that the optical absorptions around 420 and 475 nm are Ion to Ligand Charge Transfer (ILCT) bands. The UV-Vis spectra is consistent with the ion-pair of the complex measured by conductivity data.[31]

3.3 Dispersion stability

We use dispersion stability measurements to probe the LRI between nanoparticles as a function of molecular functionalization. Recently we showed that mechanically wrapped multinuclear complexes can probe the tube-tube repulsive barrier in a SWCNT dispersion.[13] Essentially, we measure the onset of aggregation as we increase the concentration of coordination complex, change the charge on the complex, and vary the nuclearity of the complexes bound to the SWCNTs. We model the aggregation data using a Maxwell-Boltzmann distribution of particle energies and an activation barrier proportional to the EDL repulsion between the tubes. These data are shown in Fig. 2 with the model fit to extract the dispersion stability X_o which is the concentration of charged complex where the amount of dispersed SWCNTs had decreased by 50%. For compounds which bind strongly and collapse the EDL effectively the X_o occurs at lower concentration. Further discussion of this technique is detailed in our previous work.[32] Our prior research has concluded that the nuclearity of the complex, as well as the charge on the complex, greatly affects the onset of aggregation.[13, 33, 34] Dispersion stability is also affected by the degree of dissociation of **+2Zn2** in DMF. Dispersion stability X_o = 14.2 ± 0.3 µM for **+2Zn2** and is approximately ten times greater than that measured for the **+2Ru2** species, 1.22 ± 0.01 µM as shown in Fig. 2. Both of these complexes have the same charge, nuclearity, and π-π stacking interactions with the SWCNTs. However, since the +2Zn2 acetate salt does not fully dissociate in DMF the dominant species only has +1 charge. This reduces the ionic strength, and the EDL around the SWCNTs does not collapse as much. These results are consistent with Sogami-Ise theory of colloid stability. An increase in ionic strength compresses the EDL of the SWCNTs, decreasing its zeta potential, causing tube-tube repulsion to diminish and promote aggregation.[35] Interestingly, the +2Zn2 hydrazone complex still binds

very effectively to the surface of the nanotubes, suggesting a significant π-π interaction between the hydrazone ligand and the SWCNT surface.

3.4 Binding of molecular spacers to SWCNTs

The amount of **+2Zn2** bound to SWCNTs was measured as q_e (mg of **+2Zn2** adsorbate / g of SWCNT adsorbent) versus time. The amount of **+2Zn2** bound to SWCNTs reached a saturation level after 2 h of incubation. Adsorption isotherms of 2 h and 5 h incubations were statistically similar. We also measured the kinetics of adsorption to probe the binding mechanism. The shortest incubation time of 10 min was limited by the speed at which the sample could be loaded into the system and reach maximum RPM for the removal of the functionalized SWCNTs. Binding kinetics were measured as a function of initial concentration C_o of the **+2Zn2** complex as shown in Fig. 3. These experiments are challenging when C_o is low and far from the onset of aggregation since the SWCNTs are still stable and difficult to fully remove from dispersion. Since the **+2Zn2** complex does not absorb in the NIR where the SWCNTs do, we corrected for any remaining SWCNTs left in the solution.

At low C_o the data show that q_t approaches the calculated q_{max} within 90 min. q_{max} is the total mg of adsorbate added per total g of SWCNT present as shown as horizontal dashed lines in Fig. 3. For each initial concentration C_o, the amount of adsorbate bound to the SWCNTs increased linearly with time as indicated by the solid lines in Fig. 3. The initial rates of adsorption were calculated from the regression of q_t vs. time. The rate of binding was independent of the number of binding sites remaining which supports an independent binding site model. Moreover, the initial rates of adsorption were determined as a function of C_o. The initial rate appears to be independent of the initial concentration of adsorbate as shown in Fig. S6

(ESI†). This pseudo-zeroth-order kinetics also supports an independent binding model of the

+2Zn2 complex onto the surface sites of the SWCNTs where $[+2Zn2] = C_o - kt$. The rate

constants $k = 7.3 \pm 0.5$ (mg/g)/min and $k = 7.1 \pm 1$ (mg/g)/min are experimentally the same for

different initial concentration $C_o = 5.71$ mg/L and $C_o = 19.0$ mg/L respectively. These kinetics

data are not consistent with common pseudo-first-order or pseudo-second-order kinetic models.[36]

The data also do not represent a diffusion limited model where q_t is proportional to $t^{1/2}$. This does

not seem to be a diffusion rate limited process. It is possible that the ion pair $[+2Zn2](Ac)^+$ must

dissociate just prior to the +2 complex binding to the SWCNTs surface (negative zeta potential).

Future studies will attempt to elucidate a detailed mechanism of adsorption.

An adsorption isotherm of the **+2Zn2** complex onto SWCNTs in DMF is shown in Fig. 4.

Samples were incubated for 2 h before the SWCNTs were removed by ultracentrifugation and

then the equilibrium concentration, C_{eq} was measured by UV-Vis spectroscopy. Equilibrium

bound adsorbate is quantified as q_e in mg of adsorbate per g adsorbent. The inset of Fig. 4 shows

a DFT geometry optimization of a divalent complex near a (7,7) SWCNT (acetate anions not

included). The aromatic region of the complex wraps around the SWCNT due to π-π stacking

interactions. The tertiary butyl group enables the complex to act as a molecular spacer keeping

the SWCNTs from aggregating to their vdW closest contact.

The adsorption data were analyzed using several common isotherm models. The data

were fit to single component Langmuir, Freundlich,[37] Langmuir-Freundlich,[38] and the modified

Brunauer-Emmett-Teller (BET)[39] isotherm for liquid phase adsorption.[2, 40, 41] The model that

best fits the **+2Zn2** adsorption data is the modified BET isotherm,

$q_e = q_m \dfrac{K_s C_{eq}}{(1-K_L C_{eq})(1-K_L C_{eq}+K_s C_{eq})}$, where q_m is the adsorbate loading of one monolayer, K_s is the

equilibrium constant for the adsorbate – SWCNT surface interaction, and K_L is the equilibrium

constant for the subsequent adsorbate layer bound to the first monolayer. The data fit by the

Langmuir, Freundlich, and Langmuir-Freundlich models is shown in Fig. S7A-C (ESI†)

respectively. Statistically, the BET model best describes our data. According to the Akaike's

Information Criterion test (AIC),[42] the Langmuir is the best of the two-parameter models with an

AIC 1250 times more likely to represent the data than the Freundlich. The BET is a statistically

more likely model than the three-parameter Langmuir-Freundlich and Langmuir by factors of

22,000 and 48,000 respectively.

The modified BET model is a three-parameter function. A non-linear least squared fit on

these parameters to the data in Fig. 4 determined q_m = 704 ± 29 mg/g, K_s = 1.1 ± 0.15 (mg/L)$^{-1}$,

and K_L = 0.017 ± 0.002 (mg/L)$^{-1}$. The value of q_m is denoted by the horizontal dashed blue line

in Fig. 4. The dashed black line illustrates the closest vdW packed monolayer that the **+2Zn2**

complex can make when π-π stacked onto a flat surface. It is surprising that we were able to

measure adsorption loading so close to this theoretical maximum $\boldsymbol{q_m^*}$ = 1057 mg/g . Since

SWCNTs are curved and are present in a distribution of tube diameters from ~0.8 nm – 1.2 nm,

it is not possible to fully cover the surface with these molecules. The dashed horizontal red line

illustrates the adsorption seemingly saturate about 920 mg/g. At 14 mg/L (18.5 µM) the

adsorbate concentration is 30% higher than the onset of aggregation concentration, and some of

the SWCNTs will begin to aggregate before they can adsorb significant amounts of the **+2Zn2**

complex. Once the SWCNTs aggregate, their surface area is no longer accessible to the large

molecular ions. This phenomenon is also observed in the kinetics data in Fig.3. At low C_o the

adsorbate loading approached q_{max} . However, when C_o = 19.0 mg/L (25 µM) the SWCNTs start

to aggregate after ~60 min since the dispersion is destabilized. This is due to the concentration

14

of the **+2Zn2** being almost twice the onset of aggregation concentration (not yet at the critical coagulation concentration). Therefore the adsorption saturates below the calculated q_{max} and well below the theoretical maximum $\boldsymbol{q_m^*}$.

We observe similar adsorption behavior for the **+2Ru2** complex binding to SWCNTs in DMF. This complex is a strong electrolyte in DMF and the fully dissociated +2 complex ion is the dominant species in solution. The adsorption isotherm for the +2Ru2 tpphz complex is shown in Fig 5. In previous work, we investigated the adsorption of a series of these complexes to SWCNTs.[20, 43] Each dinuclear complex is held together with the same tpphz bridging ligand that can π-π stack with the surface of the SWCNTs. However the heteroligands differ to adjust the net charge on the complex between +2, +3, or +4. Unlike the planar **+2Zn2** complex, the heteroligands sterically constrain the ruthenium species during the adsorption to the curved surface of the SWCNTs. In our previous work we incubated the samples for 2-3 days at very low C_o due to the slow kinetics of binding. To compare directly with our current work, the data in Fig. 5 were incubated for 2 h or 5 h. Adsorption of this molecular spacer saturates well below the calculated q_{max} for each addition of the complex. The **+2Ru2** complex binds strongly to SWCNTs, but since onset of aggregation of this complex is 1.22 ± 0.01 μM as discussed above, the tubes start to aggregate when $C_o \sim 1$ mg/L of the ruthenium complex thereby reducing their available surface area. The data in Fig. 5 were fit to Langmuir, Freundlich, and BET models. The Freundlich model does not fit these data at all. The Langmuir and BET are statistically the same with an AIC of 5 favoring the two-parameter Langmuir model. This is because K_L is essentially zero making the models equivalent with $q_m = 87 \pm 4$ mg/g and $K_s = 3.5 \pm 0.6$ (mg/L)$^{-1}$. The larger binding constant K_s for the **+2Ru2** isotherm compared to the smaller $K_s = 1.1$ for the **+2Zn2** isotherm is consistent with the coulombic attraction of the fully

dissociated ruthenium species to the negative zeta potential on the SWCNTs and the more delocalized π orbitals on the bridging ligand of **+2Ru2** complex.

Elemental analysis obtained by EDX, confirmed the presence of zinc, oxygen, and nitrogen in the sample of SWCNTs. At high C_o = 19 µg/g **+2Zn2** the mass % of Zn was measured to be 4.3 ± 0.6 %w, while the expected value is 16 %w. At low C_o = 0.76 µg/g **+2Zn2** the mass % of Zn was measured to be 0.12 %w, while the expected value is 1.4 %w. The experimental values of the elemental analysis are only qualitative due to matrix effects from the sample and microscopy substrate. The trend of high %w Zn bound to the SWCNTs at higher C_o is clear.

3.5 Lower membrane resistance and higher specific capacitance

As molecular spacers intercalate between SWCNTs, they should increase ion accessible SSA and increase solvent flux through condensed thin films. According to Darcy's law,[44] the membrane resistance can be determined by: $\kappa_m = \frac{a\Delta P}{\mu Q}$ where a is the area of the membrane, ΔP is the differential pressure across it while solvent with dynamic viscosity µ is pushed through at a flow rate of Q.[45] This model describes nanofiltration membranes[46] with pore sizes on the order of 1 nm like the spacing between SWCNTs in our films. In Fig. 6 we show baseline normalized membrane resistance data for pristine SWCNTs (black diamond) and **+2Zn2** functionalized SWCNTs (triangles). Film compression after solvent drying is expected and observed after the first rinse through the pristine SWCNT film. For all hydrazone complex functionalized films, the membrane resistance increased after successive DMF rinses until reaching a stable resistance similar to the pristine film. Based on molecular mechanics calculations (COMPASS FF, dielectric constant = 36.7) of tube-tube collapse we show, in Fig. S8 (ESI†), that as the

perpendicular distance between tubes decreases, or the axial distance between molecular spacers increases, the tubes will collapse to their vdW equilibrium distance which will restrict solvent flow and ion mobility through the film. DFT cluster geometry optimization shown in Fig. S9 (ESI†) illustrates the hydrazone complex-acetate ion-pair mechanically distort around the SWCNT with a ligand-SWCNT inter-planar distance of 0.38 nm. This is slightly larger than the vdW inter-planar distance expected between two graphene sheets, 0.33 nm. The steric bulk of the *tert*-butyl group on the hydrazone ligand increases the tube-tube spacing to about 0.8 nm. The increase in membrane resistance in the hydrazone functionalized films as the complex is slowly rinsed from the SWCNT walls is consistent with this molecular spacer model.

Preliminary capacitance measurements of the functionalized SWCNT films also support a molecular spacer model. In fig. S9A-B we illustrate the DFT geometry optimization of the ion-complex-SWCNT cluster in DMF. These calculations suggest that electron density can easily be transferred between the SWCNTs and the hydrazone ligands. This can result in additional fast faradaic pseudo-capacitance. The ion accessible surface area of the SWCNTs was probed by measuring the EDL capacitance using galvanostatic charge-discharge (CD) measurements. The specific capacitance, based on SWCNT mass only, increased by 20 – 40 % for the hydrazone functionalized thin films with q = 348 mg/g. Specifically, when we discharged the film from 2 V to 0 V at 3.7 A/g in 1.0 M TBATFB in propylene carbonate electrolyte, the capacitance increased from 72.8 F/g in the pristine film to 100.5 F/g in the functionalized film. This equates to a specific energy storage E_s = 112 Wh/kg which is comparable to commercial Li ion batteries and a specific power density of 21 kW/kg, which is 100 times larger than that for a Li ion battery. While this is not an electric-energy storage paper we present this result to support the molecular spacer model described above.

4   Conclusions

We have presented an experimental study of the kinetics and equilibrium of novel coordination compounds interacting with SWCNTs in dispersion and in condensed thin films. A comparison of two separate divalent, dinuclear metal coordination complexes finds significant differences in the dispersion stability, binding kinetics, and adsorption isotherm. This paper is based on our previous reports where dinuclear ruthenium complexes show molecular spacer behavior as they intercalate between aggregating SWCNTs. Those previous studies showed significant increase in the specific capacitance of the ruthenium complex functionalized films. These materials are needed if we are to develop high power electric energy storage materials for supercapacitor devices. This current study moves away from expensive metals to develop electroactive molecular spacers from sustainable earth abundant materials. The zinc hydrazone complex binds to the SWCNTs at very high loading following a zeroth order independent binding site model. This complex does not bind as strongly as the ruthenium complexes likely because of the less extensive π conjugation around the ligand. The binding constant needs to be higher in order to enable materials with long and stable charge-discharge cycling life.

All of our data is consistent with a molecular spacer model of tube-complex-tube LRI that can lead to a controlled/directed assembly of nanostructured materials. Future studies will include TEM, XRD, and SAXS data that can measure the intertube spacing as a function of complex loading. Continued synthetic efforts should lead to spacers that bind more strongly (improved stability), have more steric bulk (increase intertube spacing and ion accessible surface area), and more facile electroactive ligands (enhanced pseudocapacitance).

5   Acknowledgements

References

1.   Yu Li, Zheng-Yi Fu and Bao-Lian Su, *Adv. Funct. Mater.*, 2012, **22**, 4634-4667.

2.   Amir Mirzaei, Amanollah Ebadi and Peyman Khajavi, *Chemical Engineering Journal*, 2013, **231**, 550-560.

3.   Nathan Behm, Dylan Brokaw, Colton Overson, Derek Peloquin and Jordan C. Poler, *J. Mater. Sci.*, 2013, **48**, 1711-1716.

4.   Pablo A. Denis, *Chemical Physics*, 2008, **353**, 79-86.

5.   Qifeng Zhang, Evan Uchaker, Stephanie L. Candelaria and Guozhong Cao, *Chemical Society Reviews*, 2013, **42**, 3127-3171.

6.   C. Richard, F. Balavoine, P. Schultz, T. W. Ebbesen and C. Mioskowski, *Science*, 2003, **300**, 775-778.

7.   J. Chen, H. Y. Liu, W. A. Weimer, M. D. Halls, D. H. Waldeck and G. C. Walker, *J. Am. Chem. Soc.*, 2002, **124**, 9034-9035.

8.   K. K. Kim, S. M. Yoon, J. Y. Choi, J. Lee, B. K. Kim, J. M. Kim, J. H. Lee, U. Paik, M. H. Park, C. W. Yang, K. H. An, Y. S. Chung and Y. H. Lee, *Adv. Funct. Mater.*, 2007, **17**, 1775-1783.

9.   J. L. Stevens, A. Y. Huang, H. Q. Peng, L. W. Chiang, V. N. Khabashesku and J. L. Margrave, *Nano Letters*, 2003, **3**, 331-336.

10.   A. Carrillo, J. A. Swartz, J. M. Gamba, R. S. Kane, N. Chakrapani, B. Q. Wei and P. M. Ajayan, *Nano Letters*, 2003, **3**, 1437-1440.

11.   Ming Zheng, Anand Jagota, E. D. Semke, B. A. Diner, R. S. McLean, S. R. Lustig, R. E. Richardson and N. G Tassi, *Nature Materials*, 2003, **2**, 338-342.

12.   D. Nepal, J. I. Sohn, W. K. Aicher, S. Lee and K. E. Geckeler, *Biomacromolecules*, 2005, **6**, 2919-2922.

13.   A. A. Ameen, A. N. Giordano, J. R. Alston, M. W. Forney, N. P. Herring, S. Kobayashi, S. G. Ridlen, S. S. Subaran, T. J. Younts and J. C. Poler, *PCCP Phys. Chem. Chem. Phys.*, 2014, **16**, 5855-5865.

14.   B. V. Derjaguin, ed. . Plenum Publishing Corporation, New York, Editon edn., 1989, p. 174.

15.   E. J. W Verwey and J. Theodoor G. Overbeek, *Theory of the stability of lyophobic colloids*, Elsevier, Amsterdam, 1948.

16.   K. Yang and B. S. Xing, *Environmental Pollution*, 2009, **157**, 1095-1100.

17.   Suzana Gotovac, Hiroaki Honda, Yoshiyuki Hattori, Kunimitsu Takahashi, Hirofumi Kanoh and Katsumi Kaneko, *Nano Letters*, 2007, **7**, 583-587.

18.   Hoon Hyung and Jae-Hong Kim, *Environmental Science & Technology*, 2008, **42**, 4416-4421.

19.   Harsh Chaturvedi, Andrea N. Giordano, Mahn-Jong Kim, Frederick M. MacDonnell, Sarah S. Subaran and Jordan C. Poler, *J. Phys. Chem. C*, 2009, **113**, 11254-11261.

20.   J. R. Alston, S. Kobayashi, T.J. Younts and J. C. Poler, *Polyhedron*, 2010, **29**, 2696 - 2702.

21.   L. D. Popov, I. N. Shcherbakov, S. I. Levchenkov, Y. P. Tupolova, V. A. Kogan and V. V. Lukov, *Journal of Coordination Chemistry*, 2008, **61**, 392-409.

22.   S. I. Levchenkov, L. D. Popov, I. N. Shcherbakov, G. G. Aleksandrov, A. A. Tsaturyan, S. S. Beloborodov, O. V. Maevskii and V. A. Kogan, *Russian Journal of Coordination Chemistry*, 2013, **39**, 493-499.

23.   V. V. Lukov, Yu P. Tupolova, V. A. Kogan and L. D. Popov, *Russian Journal of Coordination Chemistry*, 2003, **29**, 335-338.

24.   Y. Zhao and D. G. Truhlar, *Journal of Chemical Theory and Computation*, 2005, **1**, 415-432.

25.   Wenjie Fan, Jun Zeng and Ruiqin Zhang, *Journal of Chemical Theory and Computation*, 2009, **5**, 2879-2885.

26.   Haruhisa Kato, Ayako Nakamura and Masanori Horie, *RSC Advances*, 2014, **4**, 2129-2136.

27.   Adeyemi S. Adeleye and Arturo A. Keller, *Water Research*, 2014, **49**, 236-250.

28.   Gopannagari Madhusudana, Bakaraju Vikram and H. Chaturvedi, *Materials Research Express*, 2015, **2**, 075012.

29.   H. Hu, A. P. Yu, E. Kim, B. Zhao, M. E. Itkis, E. Bekyarova and R. C. Haddon, *J. Phys. Chem. B*, 2005, **109**, 11520-11524.

30.   W. Z. Ostwald, *Phys. Chem.*, 1889, **3**, 588-602.

31.   Binita Suthar, Anuar Aldongarov, Irina S. Irgibaeva, Mitra Moazzen, Bernadette T. Donovan-Merkert, Jon W. Merkert and Thomas A. Schmedake, *Polyhedron*, 2012, **31**, 754-758.

32.   Michael W. Forney, Joshua S. Anderson, Anjail L. Ameen and Jordan C. Poler, *The Journal of Physical Chemistry C*, 2011, **115**, 23267-23272.

33.   H. Chaturvedi and J. C. Poler, *J. Phys. Chem. B*, 2006, **110**, 22387-22393.

34.   Michael W. Forney and Jordan C. Poler, *The Journal of Physical Chemistry C*, 2011, **115**, 10531-10536.

35.   Wen Liu, Weiling Sun, Alistair G. L. Borthwick and Jinren Ni, *Colloids and Surfaces A: Physicochemical and Engineering Aspects*, 2013, **434**, 319-328.

36.   Mukosha Lloyd, Onyango S. Maurice, Ochieng Aoyi and Taile Y. Leswifi, *Journal of Chemistry*, 2015.

37.   A. Erto, R. Andreozzi, F. Di Natale, A. Lancia and D. Musmarra, in *Icheap-9: 9th International Conference on Chemical and Process Engineering, Pts 1-3*, ed. S. Pierucci, Editon edn., 2009, vol. 17, pp. 293-298.

38.   David G. Kinniburgh, *Environmental Science & Technology*, 1986, **20**, 895-904.

39.   Stephen Brunauer, P. H. Emmett and Edward Teller, *J. Am. Chem. Soc.*, 1938, **60**, 309-319.

40.   Fouad Jaafar and Stanislaw Michaíowski, *Drying Technology*, 1990, **8**, 811-827.

41.   Amanollah Ebadi, JafarS Soltan Mohammadzadeh and Anvar Khudiev, *Adsorption*, 2009, **15**, 65-73.

42. Hamparsum Bozdogan, *Psychometrika*, 1987, **52**, 345-370.

43. Jeffrey R. Alston and Jordan C. Poler, in *Mater. Res. Soc. Symp. Proc.*, Editon edn., 2011, vol. 1303, pp. 185 - 191.

44. Henry Darcy, in *Les Fontaines Publiques de la Ville de Dijon*, ed. V. DALMONT, Bookseller of the Imperial Corps of Bridges, Roads and Mines, Paris, France, Editon edn., 1856.

45. John C. Crittenden, R. Rhodes Trussell, David W. Hand, Kerry J. Howe and George Tchobanoglous, *MWH's Water Treatment: Principles and Design*, 3rd edn., Wiley, 2012.

46. B. Van der Bruggen, J. Geens and C. Vandecasteele, *Chemical Engineering Science*, 2002, **57**, 2511-2518.
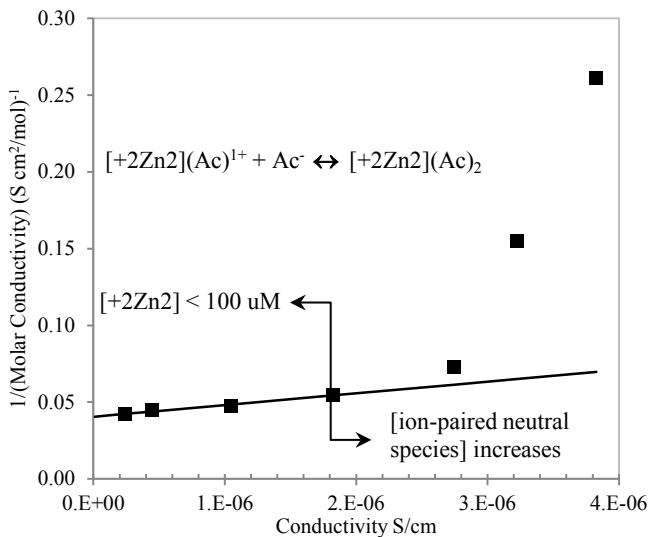
Figure 1: Ostwald's dilution law for weak electrolytes of the **+2Zn2** acetate complex in DMF. Measured limiting molar conductivity (reciprocal of the intercept of the solid line) is only a fraction of expected fully dissociated species. Monovalent species dominates at low concentration where ion-pairing results in neutral species at higher concentration.
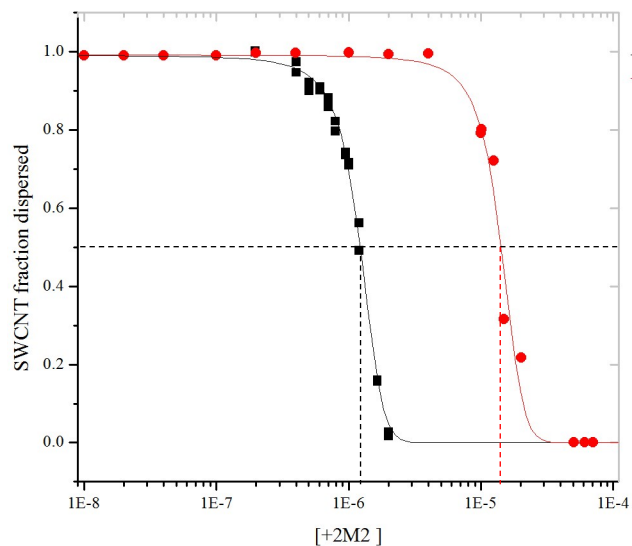
Figure 2: Onset of aggregation data for SWCNTs in DMF after 48 h. +2Zn2 hydrazone complex (red circle) has a dispersion stability of 14.2 ± 0.3 µM while that for the +2Ru2 complex (black square) is 1.22 ± 0.01 µM as determined by fit to the model (solid lines).
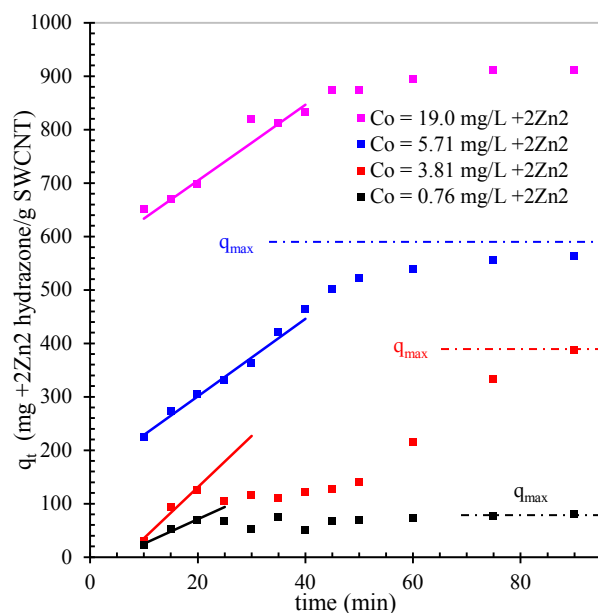
Figure 3: Adsorption Kinetics of **+2Zn2** on SWCNTs dispersed in DMF. As initial concentration C_o of the adsorbate increases the amount of complex bound q_t increases until saturation. Initial adsorption rates are constant in time (solid lines). Initial rates are quasi-independent of adsorbate concentration. Theoretical q_{max} from each C_o is marked by dashed line.
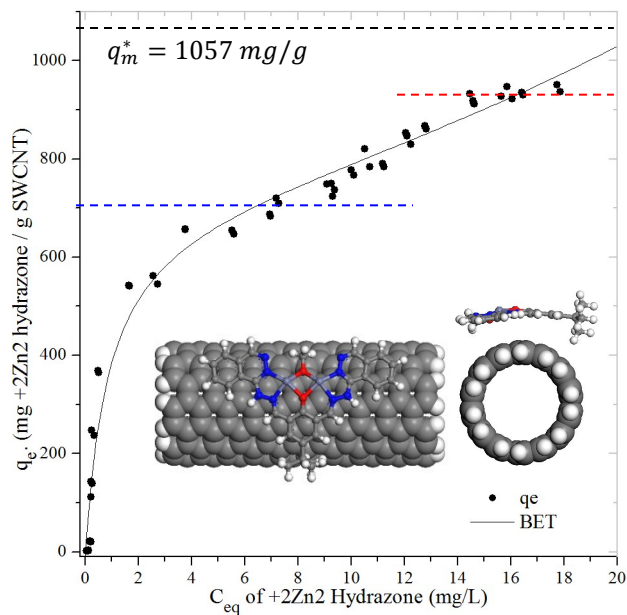
Figure 4: Adsorption isotherm of +2Zn2 hydrazone onto a SWCNT dispersion in DMF. Equilibrium concentration, C_{eq} of adsorbate is measured after SWCNT adsorbent is removed by centrifugation. Theoretic maximum packing q_m^* of adsorbate to adsorbent is indicated by dashed line. DFT optimization of hydrazone bound to (7,7) SWCNT is shown in inset.
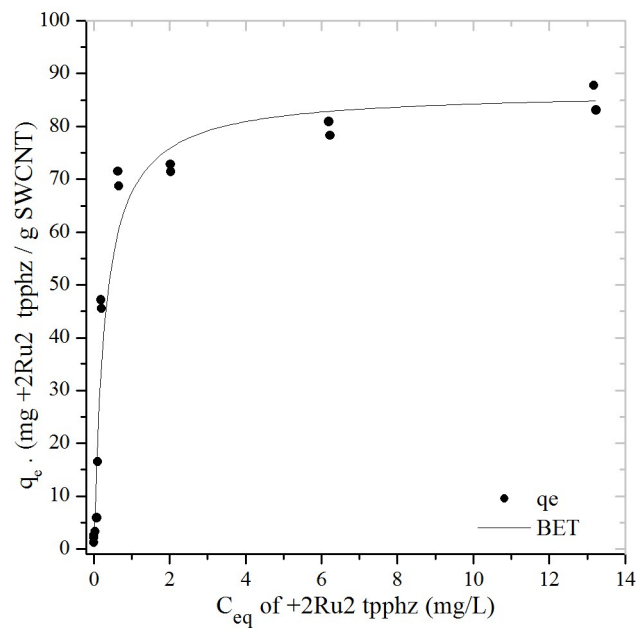
Figure 5: Adsorption isotherm of +2Ru2 tpphz onto a SWCNT dispersion in DMF. Equilibrium concentration, C_{eq} of adsorbate is measured after SWCNT adsorbent is removed by centrifugation. Langmuir and BET model identical. $q_m = 87 \pm 4$ mg/g and $K_s = 3.5 \pm 0.6$ (mg/L)$^{-1}$.
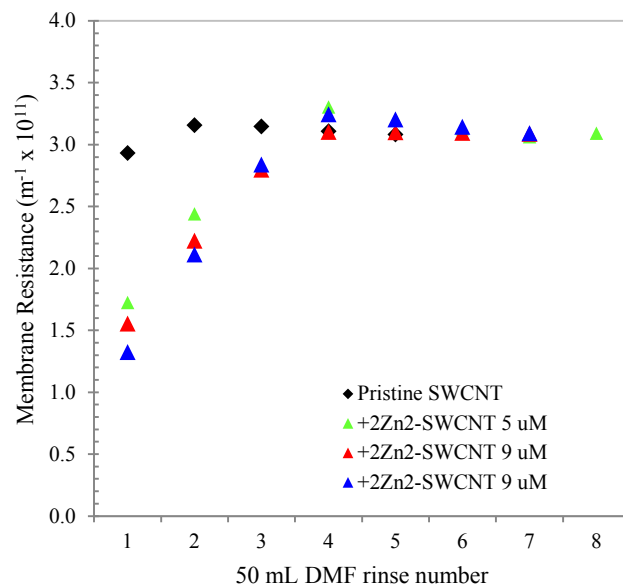
Figure 6: Membrane Resistance of thin SWCNT films. Pristine film (diamond) shows stable flow resistance after initial film compression. **+2Zn2** functionalized SWCNTs (triangles) show low membrane resistance during first few solvent rinses as molecular spacers desorb from the SWCNTs.